IEEE Access
Multidisciplinary | Rapid Review | Open Access Journal

Received March 6, 2019, accepted April 7, 2019, date of publication April 26, 2019, date of current version May 14, 2019.

Digital Object Identifier 10.1109/ACCESS.2019.2913042

Robust Virtual Inertia Control of a Low Inertia Microgrid Considering Frequency Measurement Effects

THONGCHART KERDPHOL, (Member, IEEE), FATHIN SAIFUR RAHMAN, (Student Member, IEEE), MASAYUKI WATANABE, (Member, IEEE), AND YASUNORI MITANI, (Member, IEEE)

Department of Electrical and Electronic Engineering, Kyushu Institute of Technology, Kitakyushu 804-8550, Japan

Corresponding author: Thongchart Kerdphol (kerdphol@ele.kyutech.ac.jp)

This work was supported by the Power System and Renewable Energy Laboratory (Mitani-Watanabe Labs), Kyushu Institute of Technology, Kitakyushu, Fukuoka, Japan.

ABSTRACT Virtual inertia emulation could be regarded as an inevitable component of microgrids with renewable energy, enhancing microgrid inertia and damping properties. In applying this control technique, a phase-locked loop (PLL) is necessary to obtain the estimation of the system frequency data. However, the employment of PLL could cause larger frequency oscillation to the microgrid due to its dynamics. This issue would be exacerbated in a low-inertia microgrid driven by high renewable penetration, severely deteriorating the frequency stability. Thus, the effect of PLL with measurement delay is a critical issue in utilizing the virtual inertia control. To overcome such problem, this paper proposes a robust virtual inertia control for a low-inertia microgrid to minimize the undesirable frequency measurement effects, improving the microgrid frequency stability. The robust H_∞ control design using a linear fractional transformation (LFT) technique is used to develop the virtual inertia control loop, considering the dynamics of PLL with measurement delay and the uncertainties of system inertia and damping. The efficacy of the proposed H_∞ control method is compared to the conventional and optimum proportional-integral (PI)-based inertia control. The results show that the H_∞-based robust virtual inertia control is superior to both conventional virtual inertia control and optimum PI-based virtual inertia control against a wide range of microgrid operating conditions, disturbances, and parametric uncertainties.

INDEX TERMS Frequency stability, H_∞ control, inertia control, microgrid, renewable energy, virtual synchronous generator.

I. INTRODUCTION

Currently, integration of renewable energy sources (RESs) into the conventional synchronous generator-based power system is rapidly increasing due to environmental concern, economic growth, and energy crisis. The microgrid, as a new small-scale power system concept, is suitable for integrating RESs into the distribution system [1]. Accordingly, RESs become the highly-shared structures in the microgrid. However, the high RESs penetration could lead to serious frequency stability issues in the microgrid. Firstly, a high RESs integration reduces the number of traditional generation units which can provide the reserve power for primary/secondary control, leading to higher frequency deviation and weakening of microgrid stability. Secondly, the RESs-based generation typically has non-existent or low inertia due to the employment of power electronics interfaces. Consequently, the RESs-based generation could not participate in frequency regulation in normal microgrid operation [2]. Hence, integrating RESs into the microgrid will significantly decrease the total system inertia. The reduction in system inertia will lead to an increased rate of change of frequency (ROCOF), causing rapid and severe changes in system frequency, even at a small disturbance. These issues may lead to microgrid instability and blackout.

In response to the stability challenges caused by low system inertia due to high RESs penetration, new concepts for virtual inertia emulation (i.e., virtual synchronous generator/machine) have been proposed to supply an additional virtual inertia into the microgrid, allowing a high RESs

The associate editor coordinating the review of this manuscript and approving it for publication was Lifeng Ma.

participation in microgrid operation [3]–[5]. The virtual inertia is imitated using an advanced control of the inverter and energy storage system (ESS), enhancing system inertia, damping properties, and frequency stability [6], [7]. Past achievements and literature reviews on virtual inertia control and its application are provided in [2], [8]. [9] confirmed that the application of virtual inertia control could provide uninterruptable power transfer between islanded and grid-connected modes, increasing frequency stability/resiliency of microgrids.

In real practice, the frequency measurement device such as a phase-locked loop (PLL) is very important for the application of power electronics-based converter/inverter. Owing to the use of the inverter, virtual inertia control techniques will require a PLL for frequency estimation and grid frequency synchronization. Hence, the ability of virtual inertia control to react to the rapid system frequency variations depends on the frequency measurement [8]. However, the utilization of PLL with measurement delay has some drawbacks, such as harmonics and noise. It could also lead to a higher frequency/voltage oscillation due to its dynamics [10]. The PLL effects are even more severe in low inertia microgrid with high RESs penetration and could lead to system instability and failure. Recently, the effects of PLL in virtual inertia control application on frequency stability are investigated in [11], confirming that the PLL dynamics is one of the critical issues in utilizing virtual inertia control and maintaining stable operation of power system.

Several research works on virtual inertia control are provided in [2]–[9]. In those works, the effect of frequency measurement, which is important for microgrid/inertia control, has not been considered. Moreover, the uncertainty formulation has not been designed. Hence, it is tough to confirm simultaneous robust performance and stability in a wide range of microgrid operating conditions, especially in low inertia microgrid. In the presence of uncontrollable uncertainties (i.e., system inertia, damping properties, intermittent power of RESs, and the effects of frequency measurement), microgrid becomes highly nonlinear and hence, virtual inertia control performance might be inadequate for microgrid operation and control. According to the possibility of uncertainty formulation in the control synthesis process [12], several uncertainties could be easily considered by using robust control techniques and thus, such problems could be effectively solved. The application of robust control techniques for virtual inertia control has been investigated in a few studies. Reference [13] proposed a robust virtual inertia control considering system inertia and damping as the uncertainties. Reference [14] presented the optimal tuning parameters of virtual inertia control using the robust control technique. However, the previous works in [13], [14] neglect the dynamics of frequency measurement in virtual inertia control design. As mentioned in [8], the performance of the virtual inertia control is directly influenced by the dynamics of the frequency measurement device. Since the dynamics of the frequency measurement device is neglected in their design, the previous robust control designs may be insufficient and unstable in real practice. To the best of our knowledge, there is no investigation on the robust control technique for virtual inertia control that assures the system stability by also considering the effects of the frequency measurement device.

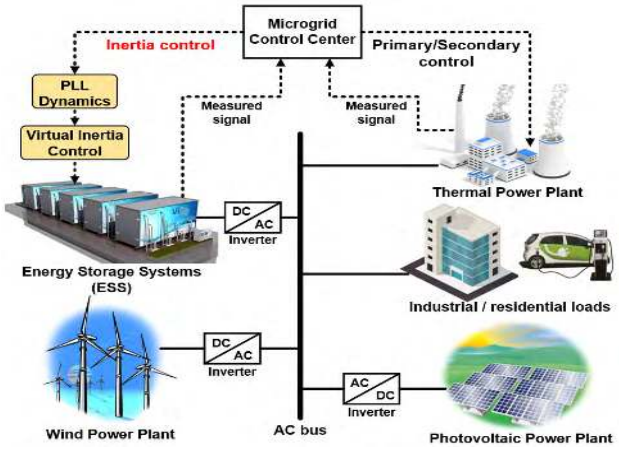

FIGURE 1. A schematic diagram of the islanded microgrid.

Considering the importance of frequency measurement in virtual inertia control, this work addresses the implementation of robust virtual inertia control of a low inertia microgrid by taking into account the effect of frequency measurement and considering it as one of the uncertainties and thus, improving frequency stability/performance. The virtual inertia control is constructed using the derivative control technique [6], [7], [11]. The robust H_∞ control method is flexible enough to combine important uncertainties such as system inertia, damping properties, and the dynamics of PLL with measurement delay in the control synthesis process. For the robust H_∞ control design, a linear fractional transformation (LFT) is implemented to develop the virtual inertia control loop. The parametric perturbation has been lumped into one block, representing the uncertainty. The efficiency and robustness of the proposed control technique are compared with an optimum PI-based virtual inertia control and a conventional virtual inertia control.

The main contribution/novelty of the robust H_∞ control technique in this work over the current methods is summarized as: (1) treating the effects of PLL and delayed measurement, system inertia, and damping properties as a bounded region of uncertainties in the H_∞ control design process; (2) treating the effects of high renewable integration/load consumption as a bounded region of disturbances in the H_∞ control design process; (3) the effects of frequency measurement have been considered in the design of the robust H_∞-based virtual inertia controller to diminish the undesirable effects of frequency measurement. Compared to the system with conventional inertia control

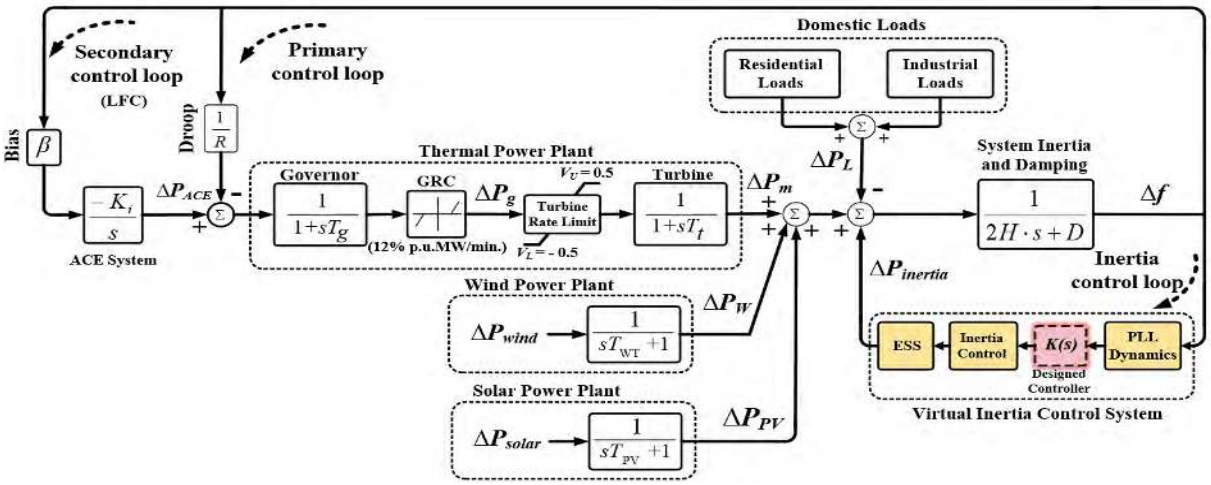

FIGURE 2. A dynamic structure of the microgrid for frequency stability analysis.

(designed in [6], [7], [11]) equipped with PLL and the system with the PI controller-based virtual inertia control equipped with PLL, the proposed robust H_∞-based virtual inertia control offers remarkable stability and performance in reducing frequency excursion/transient and maintaining frequency fluctuation close to zero. Accordingly, the dynamic effects of utilizing a frequency measurement device could be effectively solved, improving frequency stability and avoiding instability and power blackout.

II. SYSTEM MODELING

A. STRUCTURE OF THE STUDIED MICROGRID

To demonstrate practical dynamics of a microgrid, the studied microgrid consists of various types of generation and load including 12 MW of thermal power plant (i.e., conventional synchronous generation), 7 MW of wind power plant, 6 MW of photovoltaic power plant, 4 MW of energy storage system (ESS), 5 MW of residential loads, and 10 MW of industrial loads (See Fig. 1). 15 MW represents the system base. The power line (solid line) is used for trading the required electrical power, while the communication line (dash line) is used for trading control and status information.

To conduct the frequency stability analysis, the dynamic structure of the studied system considering the dynamic effects of virtual inertia control with frequency measurement is constructed as in Fig. 2. The values of control parameters are listed in Table 2 in Appendix. Based on [12], [15], the low-order dynamic model constructured in this study is accurate enough for analyzing frequency stability issues. To realize the practical aspect of the microgrid, the generator rate constraint (GRC) of the governor unit and the limitation of the rate of valve gate closing/opening (V_u, V_L) of the turbine unit are considered, extensively creating system non-linearity. The thermal power plant generates the required power for supplying domestic loads and provides primary frequency control. The area control error (ACE) system is applied to eliminate the steady-state frequency error for secondary frequency control. The ESS generates the inertia power for the virtual inertia control loop. The renewable generations such as solar and wind systems are controlled to inject the renewable power into the microgrid. However, they are not participating in frequency control. Hence, the renewable generations and domestic loads, such as industrial and residential loads, are defined as the external disturbances to the studied microgrid.

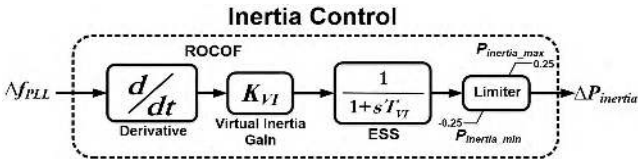

FIGURE 3. A dynamic structure of the virtual inertia control.

B. STRUCTURE OF VIRTUAL INERTIA CONTROL WITH FREQUENCY MEASUREMENT EFFECTS

Virtual inertia control [2]–[9] is introduced to imitate the inertia/damping properties of the synchronous generation, enhancing microgrid stability and allowing a high share of RESs participation in the microgrid. In this study, the derivative control technique [6], [7], [11] is applied to evaluate the ROCOF for adjusting the active power of ESS to the set-point value of the system after the disturbance. Thus, the virtual inertia is emulated by using the combination of a phase-locked loop (PLL), derivative control technique, and inverter-based ESS. The dynamic structure of virtual inertia control is presented in Fig. 3. To obtain the actual dynamic characteristics of the ESS, the low-pass filter is used in the control system. The filter is able to remove the noise issue caused by the employment of PLL. To simulate the practical energy response of the ESS, the limiter block is applied for restricting the maximum/minimum energy capacity of

the ESS. By using virtual inertia control, the ESS could be controlled to supply the required virtual inertia power into the microgrid to improve system stability. The equation/control law of virtual inertia control is defined as:

$$\Delta P_{inertia} = \frac{K_{VI}}{1 + sT_{VI}} \left(\frac{d\left(\Delta f_{PLL}\right)}{dt} \right) \tag{1}$$

where K_{VI} is the virtual inertia control gain. T_{VI} is the time-constant of virtual inertia. Δf_{PLL} is the system frequency change measured from the PLL.

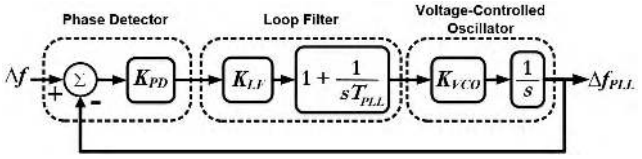

FIGURE 4. A dynamic structure of the PLL with measurement delay.

PLL is one of the techniques used for frequency measurement and grid synchronization in power electronics-based converter/inverter. Since virtual inertia control uses the power electronics converter, PLL is required in the virtual inertia control application. Thus, the ability of virtual inertia control to respond to the rapid system frequency changes depends on PLL [8]. Since the dynamics of PLL will introduce noise, delay, and overshoot to the microgrid, it is important to consider the effect of PLL dynamics in the frequency control design. The dynamics of PLL including measurement delay could be denoted by the first-order or second-order models [10]. The dynamic structure of PLL with measurement delay is displayed in Fig. 4. It mainly consists of a phase detector, loop filter, and voltage-controlled oscillator. Considering $K_{PD} = K_{VCO} = 1$, the second-order dynamic equation or control law of PLL with measurement delay can be obtained as [10], [11]:

$$\Delta f_{PLL} = \frac{K_{LF} \cdot s + K_{LF}/T_{PLL}}{s^2 + K_{LF} \cdot s + K_{LF}/T_{PLL}} \tag{2}$$

In addition, (2) can be written in the form of a normalized function as:

$$\Delta f_{PLL} = \frac{2\zeta\omega_n \cdot s + \omega_n^2}{s^2 + 2\zeta\omega_n \cdot s + \omega_n^2} \tag{3}$$

where

$$\omega_n = \frac{\sqrt{K_{LF}}}{\sqrt{T_{PLL}}} \text{ and } \zeta = \frac{\sqrt{K_{LF} T_{PLL}}}{2} \tag{4}$$

The approximated time-constant of the PLL transfer function is $\tau = 1/\zeta\omega_n$ for 1 % of steady-state response [10], where, $\omega_n = 1.5$ and $\zeta = 1/\sqrt{2}$. Δf is the system frequency change. K_{PD} is the phase-detector control gain. K_{LF} is the loop-filter control gain. K_{VCO} is the gain of the voltage-controlled oscillator. T_{PLL} is the time constant of the PLL.

In this study, the second-order function of the PLL is denoted by using a group of two-linear state equations as:

$$\begin{bmatrix} \dot{\Delta f}_{PLL1} \\ \dot{\Delta f}_{PLL2} \end{bmatrix} = \begin{bmatrix} 0 & 1 \\ -\omega_n^2 & -2\zeta\omega_n \end{bmatrix} \begin{bmatrix} \Delta f_{PLL1} \\ \Delta f_{PLL2} \end{bmatrix} + \begin{bmatrix} 0 & 0 \\ 2\zeta\omega_n & \omega_n^2 \end{bmatrix} \begin{bmatrix} \Delta f \\ \dot{\Delta f} \end{bmatrix} \tag{5}$$

Thus, considering the effect of PLL on the studied microgrid, the dynamic equations of PLL can be represented as:

$$\dot{\Delta f}_{PLL1} = \Delta f_{PLL2} \tag{6}$$

$$\dot{\Delta f}_{PLL2} = \alpha_1 \Delta f + \alpha_2 \Delta P_m + \alpha_2 \Delta P_g + \alpha_2 \Delta P_{ACE} + \alpha_2 \Delta P_{inertia} - \omega_n^2 \Delta f_{PLL1} - 2\zeta\omega_n \Delta f_{PLL2} \tag{7}$$

where

$$\alpha_1 = -2\zeta\omega_n + \omega_n^2$$

and

$$\alpha_2 = \zeta\omega_n \tag{8}$$

In addition, ΔP_m is the generated power change from the distributed generator (i.e., thermal power station). ΔP_g is the governor valve-position change. ΔP_{ACE} means the control signal change for secondary control. H means the system inertia. D is the damping property of the system.

C. RELATION BETWEEN FREQUENCY CONTROL AND INERTIA CONSTANT

For analyzing frequency regulation in the power systems, the correlation between generated power, load and frequency deviation is denoted by the well-known swing equation as [15]:

$$\Delta P_m - \Delta P_L = 2Hs\left(\Delta f\right) + D\left(\Delta f\right) \tag{9}$$

where ΔP_L is the load power change.

When system inertia (H) and/or damping property (D) decrease, the ROCOF and frequency deviation are augmented. For microgrids, the value of D is likely low, while H is mainly changing based on the number of distributed synchronous generators in the system [14]. Therefore, the relation between the inertia constant of the synchronous generation and microgrid inertia constant is expressed as [12], [15]:

$$H = \sum_i \left(H_{SGi} S_{SGi}\right) / S_{MG} \tag{10}$$

where S_{SG} and S_{MG} are the rated power of synchronous generator and total microgrid power, respectively. When the penetration of RESs increases, the system inertia significantly reduces.

III. STATE-SPACE DYNAMIC MODELING

In response to frequency stability issues caused by low microgrid inertia and frequency measurement effect, three main control processes (i.e., primary, secondary and inertia control) are applied in this paper. Based on Fig. 2, the dynamic equation of microgrid frequency deviation is expressed as:

$$\Delta f = \frac{1}{2Hs + D}(\Delta P_m + \Delta P_W + \Delta P_{PV} + \Delta P_{inertia} - \Delta P_L) \tag{11}$$

where

$$\Delta P_m = \frac{1}{1 + sT_t}\left(\Delta P_g\right) \tag{12}$$

$$\Delta P_g = \frac{1}{1 + sT_g}\left(\Delta P_{ACE} - \frac{1}{R}\Delta f\right) \tag{13}$$

$$\Delta P_{ACE} = \frac{K_i}{s}\left(\beta \cdot \Delta f\right) \tag{14}$$

$$\Delta P_W = \frac{1}{1 + sT_{WT}}\left(\Delta P_{wind}\right) \tag{15}$$

$$\Delta P_{PV} = \frac{1}{1 + sT_{PV}}\left(\Delta P_{solar}\right) \tag{16}$$

The state-space model of the dynamic microgrid is a beneficial representation for the robust/modern control scheme [12]. To evaluate the detailed analysis, the linearized state-space model representation of the studied system is defined as:

$$\dot{x} = Ax + B_1 w + B_2 u \tag{17}$$

$$y = Cx \tag{18}$$

where the state vector $x^T = [\Delta f\ \Delta P_m \Delta P_g \Delta P_{ACE} \Delta P_{inertia}\ \Delta P_W \Delta P_{PV} \Delta f_{PLL1} \Delta f_{PLL2}]^T$, the disturbance vector $w^T = [\Delta P_{wind} \Delta P_{solar} \Delta P_L]^T$, the control input $u = \Delta P_C$, the control output $y = \Delta f_{PLL}$. ΔP_C is the control signal change from the robust controller. ΔP_{wind} means the initial wind power variation. ΔP_W means the change in generated power-based wind farm. ΔP_{solar} is the initial solar power variation. ΔP_{PV} is the change in generated power-based solar farm.

Using suitable state variables and definition from (1), (5)-(16), the linearized state-space model of the studied microgrid is achieved in the form of (17) and (18) considering the effects of uncertainties and disturbances as (19), shown at the bottom of this page.

IV. ROBUST VIRTUAL INERTIA CONTROL DESIGN CONSIDERING FREQUENCY MEASUREMENT EFFECTS

In this section, the robust $H\infty$ control theory is applied to design the robust virtual inertia controller considering the dynamic effects of PLL with measurement delay and the variation in system inertia and damping. The main objective of this robust controller is to diminish frequency deviation caused by the effects of frequency measurement and the reduction in system inertia and damping, accordingly enhancing system frequency performance and stability. The designing process of the robust$H\infty$-based virtual inertia control is described in the following subsections. For more detailed information about the robust $H\infty$ control theory and proofs, interested readers can find in [12], [16].

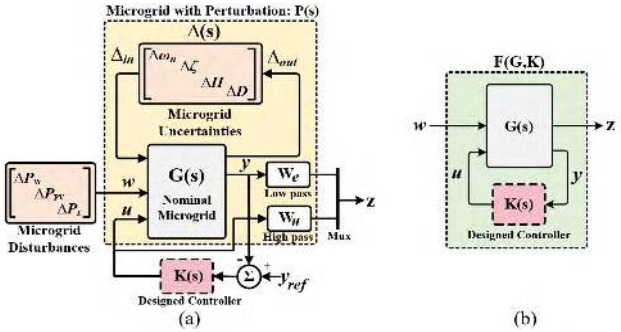

FIGURE 5. The closed-loop structure of the microgrid in the form of: (a) The lumped multiplicative disturbances and uncertainties. (b) $H\infty$ control structure.

A. UNCERTAINTY MODELING

Considering the robust $H\infty$ control framework in regards to the uncertainties, the dynamic effects of PLL with measurement delay (ω_n and ζ), system inertia (H), and damping properties (D) are considered as parametric uncertainties with $\pm 50\%$ variation. These uncertainties are extracted from the microgrid as the structured uncertainty and modeled based on a standard formation of the linear-fractional transformation (LFT) as displayed in Fig. 5(a).

$$\dot{x} = \begin{bmatrix} -\frac{D}{2H} & \frac{1}{2H} & 0 & 0 & \frac{1}{2H} & \frac{1}{2H} & \frac{1}{2H} & 0 & 0 \\ 0 & -\frac{1}{T_t} & \frac{1}{T_t} & 0 & 0 & 0 & 0 & 0 & 0 \\ -\frac{1}{RT_g} & 0 & -\frac{1}{T_g} & \frac{1}{T_g} & 0 & 0 & 0 & 0 & 0 \\ \beta \cdot K_i & 0 & 0 & 0 & 0 & 0 & 0 & 0 & 0 \\ 0 & 0 & 0 & 0 & -\frac{1}{T_{VI}} & 0 & 0 & 0 & 0 \\ 0 & 0 & 0 & 0 & 0 & -\frac{1}{T_{WT}} & 0 & 0 & 0 \\ 0 & 0 & 0 & 0 & 0 & 0 & -\frac{1}{T_{PV}} & 0 & 0 \\ 0 & 0 & 0 & 0 & 0 & 0 & 0 & 0 & 1 \\ \alpha_1 & \alpha_2 & \alpha_2 & \alpha_2 & \alpha_2 & 0 & 0 & -\omega_n^2 & -2\zeta\omega_n \end{bmatrix} x + \begin{bmatrix} 0 & 0 & -\frac{1}{2H} \\ 0 & 0 & 0 \\ 0 & 0 & 0 \\ 0 & 0 & 0 \\ 0 & 0 & 0 \\ \frac{1}{T_{WT}} & 0 & 0 \\ 0 & \frac{1}{T_{PV}} & 0 \\ 0 & 0 & 0 \\ 0 & 0 & 0 \end{bmatrix} w + \begin{bmatrix} 0 \\ 0 \\ 0 \\ 0 \\ 0 \\ 0 \\ 0 \\ \frac{K_{VI}}{T_{VI}} \\ \frac{K_{VI}}{T_{VI}} \end{bmatrix} u,$$

$$y = \begin{bmatrix} 0 & 0 & 0 & 0 & 0 & 0 & 0 & 1 & 1 \end{bmatrix} x \tag{19}$$

Nevertheless, the power changes in wind velocity (ΔP_W), solar irradiation (ΔP_{PV}),and load demand (ΔP_L) are also recognized as the main external disturbances in the control design. To evaluate an optimal $H\infty$ controller, the ∞-norm of $F(G,K)$ considering the parametric uncertainties and the external disturbances must not exceed one. $G(s)$ is the nominal microgrid model without perturbation. $P(s)$ is nominal microgrid including the dynamic perturbation. $K(s)$ represents the designed controller. z is the desired performance signal. w is the disturbance signal. Δ_{in} and Δ_{out} are the uncertainty input and output. To acquire appropriate closed-loop stability performance/margin, weighting functions (W_e and W_u) are applied to shape and normalize the control signal. W_e represents the low-pass characteristic, which affects the modeling error, frequency stability, and control output (y). W_u represents the high-pass behavior, which evaluates the weight on the control input (u). In this paper, W_e and W_u are optimally determined based on the suitable method in [16] as:

$$W_e = 20 \cdot \frac{50s + 20}{0.8s + 0.001} \tag{20}$$

$$W_u = 0.001 \cdot \frac{0.05s + 60}{10^{-5}s + 20} \tag{21}$$

B. OPTIMAL DESIGN OF H∞ CONTROLLER

The robust $H\infty$control determines a suitable robust controller to minimize the infinity (∞)-norm of $F(G,K)$ based on the LFT technique. The basic closed-loop LFT for designing the robust $H\infty$control is shown in Fig. 5(b). To obtain a suitable robust controller $K\infty$, the ∞-norm of $F(G,K)$ must not exceed one [12]:

$$\|F\ (G, K)\|_\infty < 1 \tag{22}$$

where $F(G,K)$represents the transfer function matrix of the nominal closed-loop microgrid from the disturbance input signal (w) to the desired output signal (z), which is denoted by the transfer function T_{wz}.

C. NOMINAL PERFORMANCE AND STABILITY

The nominal performance and stability are satisfied since the closed-loop T_{wz} is internally stable for the designed $K\infty$ controller. For determining the nominal stability and performance, the designed $K\infty$ controller has to satisfy the stability and performance criterion for all frequencies as [12]:

$$\left\| \begin{bmatrix} W_e\ (I + GK)^{-1} \\ W_u K\ (I + GK)^{-1} \end{bmatrix} \right\|_\infty < 1 \tag{23}$$

Using the function *hinfsyn* provided by the MATLAB® robust toolbox, the inequality equation from (23) can be determined. Fig. 6 illustrates that the infinity norm inequality of (23) is fulfilled (less than one). Therefore, it is verified that the closed-loop system efficiently removes the disturbance effects and the desired performance is well reached.

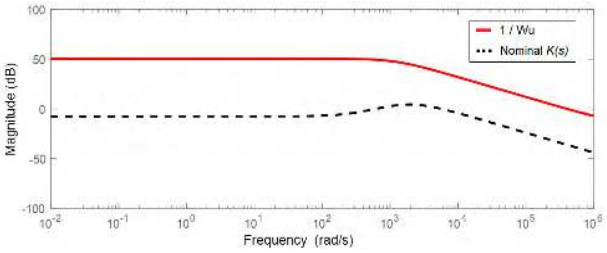

FIGURE 6. *K(s)* **of the nominal system.**

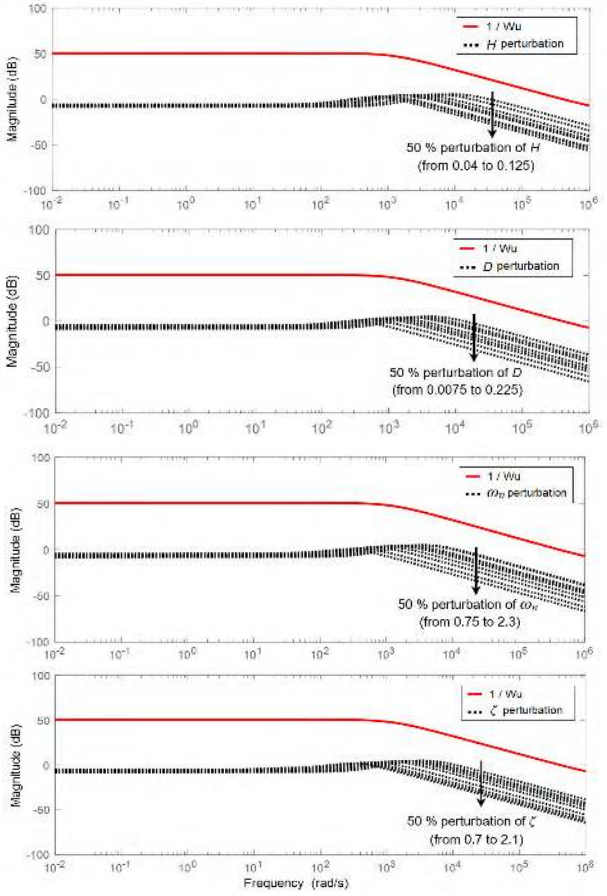

FIGURE 7. *K(s)* **of the system under various uncertainty perturbation of** ***H*****,** ***D*****,** ω_n**, and** ζ**.**

D. CLOSED-LOOP ROBUST PERFORMANCE AND STABILITY

In the modeling process of the structured uncertainty, the robust performance and stability will be satisfied if the closed-loop T_{wz} is internally stable for whole possible plants $P = (I+\Delta(s))G(s)$, where $\Delta(s)$ means the uncertainty matrix. To obtain the robust performance and stability, the designed $K\infty$ controller must fulfill the criterion for whole possible plants considering the uncertainties as [12]:

$$\left\| \begin{bmatrix} W_e\ (I + GP)^{-1} \\ W_u K\ (I + GP)^{-1} \end{bmatrix} \right\|_\infty < 1 \tag{24}$$

Fig. 7 demonstrates that the ∞-norm inequalities determined by (24) are less than one for all possible

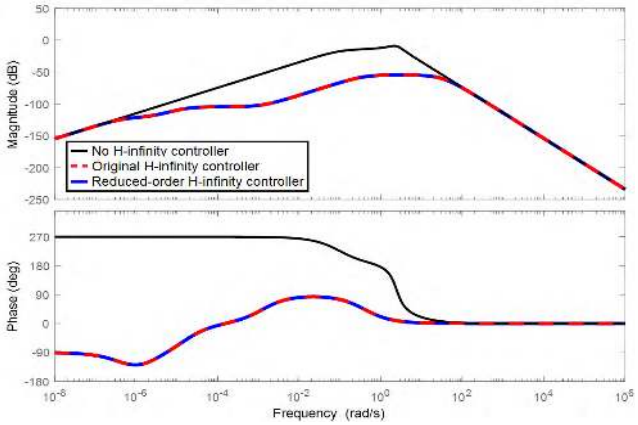

FIGURE 8. Bode plots of the reduced-order and original/full-order $H\infty$ controller.

plants. Additionally, $|||[K(I+GP)^{-1}]|||_\infty$ lower than $1/W_u$ or $|||[W_uK(I+GP)^{-1}]|||_\infty < 1$ is reached. This means that the robust performance and stability are well achieved for the $K\infty$ controller via the performance criterion of infinity norm inequality based on (24).

V. ORDER REDUCTION OF H∞ CONTROLLER

Most robust/optimal control techniques will have a high-order dynamic controller or complex state feedback, which is impractical for real-world power system implementation. To solve such problem, numerous methods have been introduced to reduce the controller order [12]. In this study, the designed $H\infty$ controller has a high-order (9th). Applying the standard Hankel norm estimation, the order can be decreased to the fourth order with no performance deterioration. Fig. 8. shows the Bode plots of the reduced and full-order$H\infty$ controllers. The designed controller with the full-order is given:

$$K(s) = \frac{b_8 s^7 + b_7 s^6 + \ldots + b_1 s + b_0}{a_9 s^9 + a_8 s^8 + a_7 s^7 + \ldots + a_1 s + a_0} \quad (25)$$

The coefficients of the designed controller in the form of (25) have been given in Table 1.

TABLE 1. The coefficients of the original $H\infty$ controller.

a_9	0.8	b_8	6.35×10^6
a_8	3107	b_7	1.73×10^9
a_7	3.12×10^6	b_6	2.32×10^{10}
a_6	4.17×10^6	b_5	7.19×10^{10}
a_5	1.17×10^8	b_4	7.35×10^{10}
a_4	9.12×10^7	b_3	3.20×10^{10}
a_3	2.44×10^7	b_2	5.94×10^9
a_2	1.66×10^6	b_1	3.40×10^8
a_1	2045	b_0	-4279
a_0	0.0048		

From Fig. 8, it is confirmed that the high-order controller is successfully reduced to a low-order controller with no performance degradation. The transfer function of the reduced-order controller can be expressed as $K(s) = N(s)/D(s)$ where:

$$N(s) = 6.35\times10^6 s^3 + 1.64\times10^9 s^2 + 6.58\times10^8 s - 8164,$$
$$D(s) = 0.8s^4 + 3096s^3 + 3.07\times10^6 s^2 + 3856s + 9\times10^{-3} \quad (26)$$

VI. RESULTS AND DISCUSSION

In this segment, the importance of employing the robust $H\infty$-based virtual inertia control to diminish the effects of frequency measurement and system inertia and damping reduction is demonstrated. To show the efficacy of the robust control, the results of the robust $H\infty$ controller (reduced-order) are compared to the optimal PI-based virtual inertia control (usually employed in real practice or industry applications) and conventional inertia control. The optimum PI-based virtual inertia control is designed using MATLAB internal-model control (IMC)-based tuning [17] and the optimum K_P and K_I are properly obtained as 18.015 and 5.473, respectively. To maintain the microgrid frequency and time deviation within the power quality point of view, the acceptable ranges of frequency operating standards used in this study are set as 49 to 51 Hz (±1 Hz) during the generation/load event, and as 49.5 to 50.5 Hz (±0.5 Hz) during no contingency event. These indexes are used in today power systems of Nordic countries and Australia [18]. To investigate the frequency stability of the microgrid in the presence of various disturbances and uncertainties, four test scenarios are considered as follows.

A. EFFECTS OF FREQUENCY MEASUREMENT ON MICROGRID STABILITY

In the first scenario, the effects of PLL with measurement delay on the microgrid performance/stability are investigated by a 10% step load change (0.1 p.u.). It is presumed that the value of ζ is fixed while the value of ω_n is varied for investigating the dynamic effect of PLL. During the normal operating condition (high system inertia) in Fig. 9(a), employing a PLL is obviously disturbing the microgrid stability, causing a larger frequency overshoot due to the zero in the numerator of its second-order model. This effect is severely exacerbated in low inertia condition as displayed in Fig. 9(b). Nevertheless, the effect of PLL on virtual inertia control can be illustrated based on the PLL time response. It is obvious that when the time constant of PLL is low (high ω_n), the actual effect of virtual inertia control could be observed. However, when the time constant of the PLL increases, the effect of virtual inertia control is significantly revoked, deteriorating the frequency stability. Thus, the robust $H\infty$-based virtual inertia controller should be applied to solve such uncertainty effects.

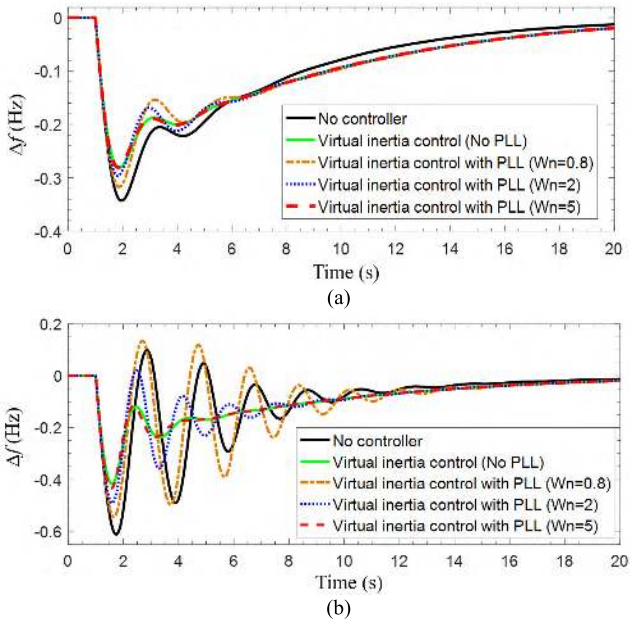

FIGURE 9. Frequency response under (a) High system inertia ($H = 100\%$) with PLL effect and (b) Low system inertia ($H = 50\%$) with PLL effect.

B. STABILITY ASSESSMENT UNDER STEP LOAD/RESs CHANGES

In the second case, the performance of the $H\infty$-based virtual inertia controller with PLL effect is investigated by various step change of loads/RESs (±0.1 p.u.) under the usual operating condition ($H = 100\%$) as shown in Fig. 10. After the sudden change of loads/RESs, a large frequency drop/overshoot occurs in case of conventional inertia control with PLL (±0.29 Hz) and no controller (±0.35 Hz). The $H\infty$-based virtual inertia control shows a superior performance in minimizing frequency deviation (±0.04 Hz) and settling-time compared to the optimum PI-based inertia control. By applying the proposed robust control, the significant improvement in frequency drop, overshoot, and ROCOF can be observed, effectively reducing the dynamic effect of PLL on microgrid stability.

C. STABILITY ASSESSMENT UNDER HIGH RESs PENETRATION

To replicate the actual microgrid operation, the variation of RESs output and loads and continuous change in system operating condition are simultaneously applied in this scenario. RESs power generation from wind/solar farms in Fig. 11(a) is highly penetrated to the system at 80% of their capacities corresponding to a 70% decrease in microgrid inertia ($H = 30\%$). To make the system condition more drastic, the residential and industrial loads in Fig. 11(b) are participating at their partial demand, resulting in low load damping and high frequency-deviation. This scenario also examines how the designed robust controller counteracts the effect of PLL in low inertia condition.

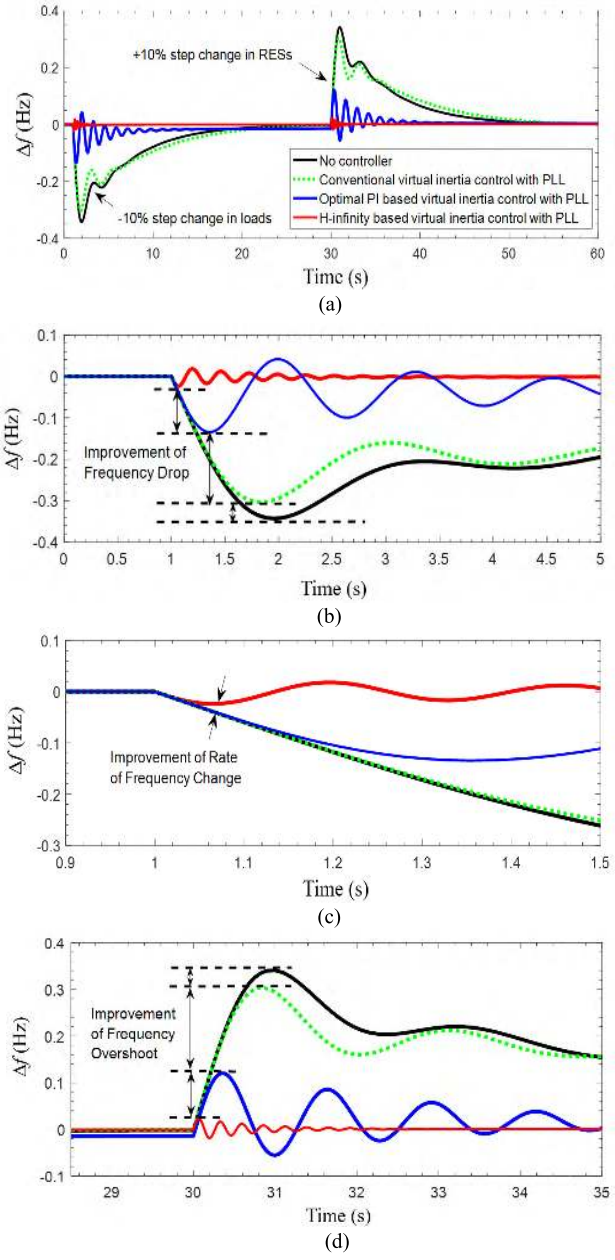

FIGURE 10. Microgrid response: (a) Frequency stability under sudden load/RESs changes. (b) Improvement of system frequency drop. (c) Improvement of ROCOF. (d) Improvement of system frequency overshoot.

Following the severe scenario with PLL effect, the microgrid frequency highly fluctuates as displayed in Fig. 12. Without virtual inertia control, the microgrid frequency widely oscillates, causing the instability and microgrid blackout. In the case of conventional virtual inertia control, the system frequency could not be maintained within the acceptable ranges of frequency operating standard, resulting in cascading failures. By applying the robust and optimum PI-based virtual inertia controllers, the system frequency could be maintained within the acceptable ranges. However, it is evident that the designed robust control regulates the system

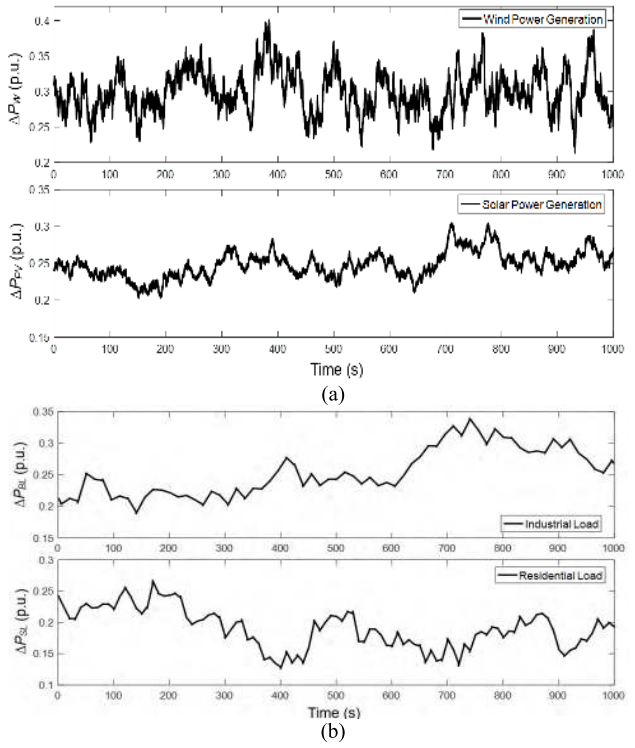

FIGURE 11. Severe disturbances for scenarios C and D: (a) Renewable power generations in the presence of high wind speed and solar irradiation, (b) Industrial and residential load demand patterns.

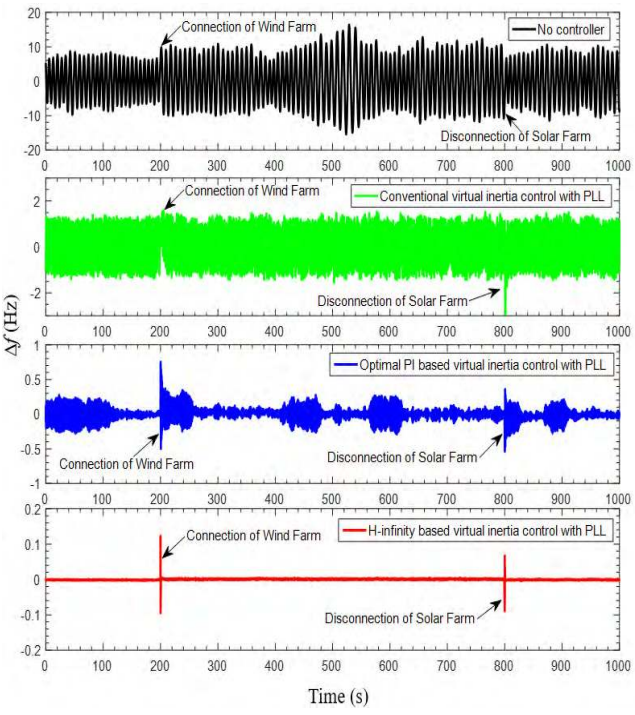

FIGURE 12. Frequency response under high RESs penetration.

frequency more effectively than the optimum PI-based virtual inertia control in terms of fast damping of oscillation with less settling time.

D. STABILITY ASSESSMENT UNDER SYSTEM UNCERTAINTIES

In real practice, microgrids could experience an inaccuracy in system parameter calculation for system design. Ultimately, the microgrid parameters may constantly change over time, degrading the system stability and performance. To investigate the robustness of the proposed robust control, the severe disturbances similar to the disturbances in Scenario C are applied while considering high parameter uncertainty with the parameter variation is provided in Table 2.

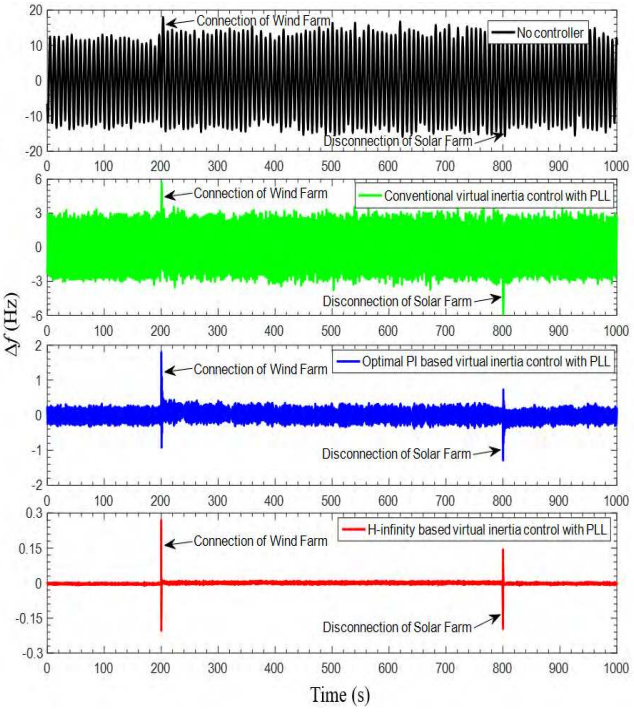

FIGURE 13. Frequency response under severe system uncertainties.

From Fig. 13, in the case of no controller and traditional virtual inertia control, the microgrid frequency is completely unstable, causing the system collapse. Clearly, the optimum PI-based inertia control also fails and cannot stabilize the microgrid frequency within the acceptable ranges, causing unstable microgrid operation. In contrast, the designed $H\infty$-based virtual inertia controller provides superior performance in minimizing frequency oscillation with smooth control effort, maintaining the security and robustness of microgrid operation. Thus, it is confirmed that the effect of uncontrollable disturbances (ΔP_W, ΔP_{PV}, ΔP_L) and uncertainties (ω_n,ζ., H, D) can be effectively suppressed by the designed robust $H\infty$-based virtual inertia controller.

From Fig. 14, the eigenvalue trajectories of the closed-loop microgrid with different control methods are evaluated against the reduction of microgrid inertia. In cases of conventional and optimum PI-based inertia controllers, the eigenvalues move toward the right side of s-planes when H is reduced.

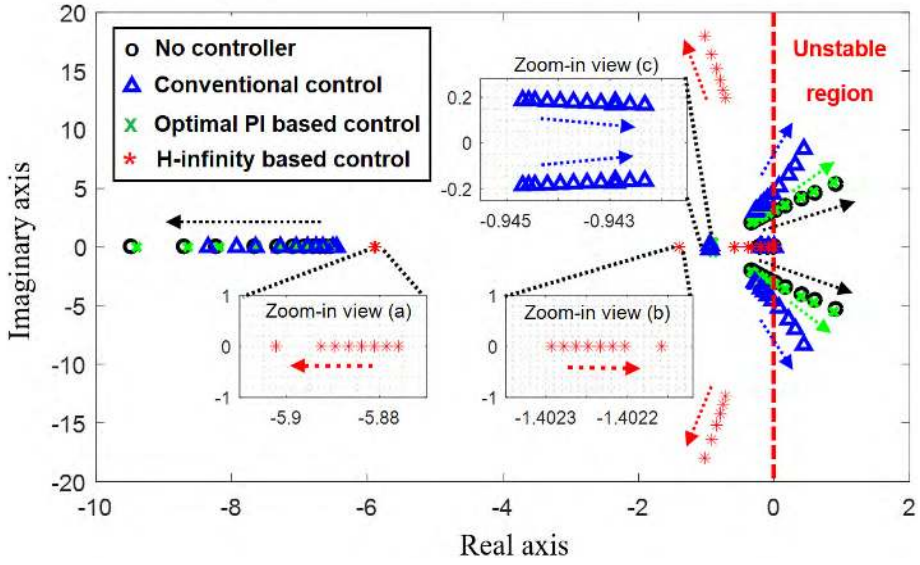

FIGURE 14. Eigenvalue paths against reducing microgrid inertia up to 90%.

TABLE 2. Dynamic parameters of studied microgrid.

Parameter	Nominal value	Scenario D (% variation)
Frequency bias factor, β (p.u.MW/Hz)	1	0.7 (-30%)
Secondary frequency controller, K_i (s)	0.05	0.03 (-40%)
Time constant of governor, T_g (s)	0.1	0.175 (+75%)
Time constant of turbine, T_t (s)	0.4	0.7 (+90%)
Droop characteristic, R (Hz/p.u.MW)	2.4	1.2 (-50%)
System damping, D (p.u.MW/Hz)	0.015	0.003 (-80%)
System inertia, H (p.u.MW s)	0.083	0.0083 (-90%)
Virtual inertia control gain, K_{VI} (s)	0.8	0.4 (-50%)
Time constant of PLL, ω_n (s)	1.5	0.3 (-80%)
Time constant of virtual inertia, T_{VI} (s)	10	11 (+10%)
Time constant of wind turbine, T_{WT} (s)	1.5	1.5
Time constant of solar system, T_{PV} (s)	1.85	1.85

In the case of the proposed robust controller, only complex eigenvalues move toward the left side of s-plane. Thus, this figure properly validates the result obtained from Fig. 13.

VII. CONCLUSION

The employment of frequency measurement devices such as the PLL in virtual inertia control could cause stability issues in a microgrid due to its dynamics. This circumstance will be even worse in the case of the microgrid with high RESs penetration, which suffers from a huge reduction of system inertia. To minimize the undesirable effects of PLL and its measurement delay in such circumstance, this work introduces the robust virtual inertia control of a low inertia microgrid, enhancing the system stability. The simulation results verify that the robustness and the stabilizing performance of the robust $H\infty$-based virtual inertia control are superior to those of the conventional and optimum PI-based virtual inertia control over various disturbances, parametric uncertainties, and system operating conditions. As revealed in the performed severe test scenarios, the proposed robust $H\infty$-based virtual inertia control loop could provide an important effect to enhance the microgrid stability and to widen the stable region, preserving the robustness of the system operation.

Appendix

See Table 2.

REFERENCES

[1] D. E. Olivares *et al.*, "Trends in microgrid control," *IEEE Trans. Smart Grid*, vol. 5, no. 4, pp. 1905–1919, Jul. 2014.

[2] M. Dreidy, H. Mokhlis, and S. Mekhilef, "Inertia response and frequency control techniques for renewable energy sources: A review," *Renew. Sustain. Energy Rev.*, vol. 69, no. 1, pp. 144–155, Mar. 2017.

[3] H.-P. Beck and R. Hesse, "Virtual synchronous machine," in *Proc. 9th Int. Conf. Elect. Power Qual. Utilisation (EPQU)*, Oct. 2007, pp. 1–6.

[4] J. Driesen and K. Visscher, "Virtual synchronous generators," in *Proc. 21st IEEE Power Energy Soc. Gen. Meeting, Convers. Del. Elect. Energy (PES)*, Jul. 2008, pp. 1–3.

[5] Q.-C. Zhong and G. Weiss, "Synchronverters: Inverters that mimic synchronous generators," *IEEE Trans. Ind. Electron.*, vol. 58, no. 4, pp. 1259–1267, Apr. 2011.

[6] E. Rakhshani, D. Remon, A. M. Cantarellas, and P. Rodriguez, "Analysis of derivative control based virtual inertia in multi-area high-voltage direct current interconnected power systems," *IET Gener. Transmiss. Distrib.*, vol. 10, no. 6, pp. 1458–1469, Apr. 2016.

[7] E. Rakhshani, D. Remon, A. M. Cantarellas, J. M. Garcia, and P. Rodriguez, "Virtual synchronous power strategy for multiple HVDC interconnections of multi-area AGC power systems," *IEEE Trans. Power Syst.*, vol. 32, no. 3, pp. 1665–1677, May 2017.

[8] H. Bevrani, T. Ise, and Y. Miura, "Virtual synchronous generators: A survey and new perspectives," *Int. J. Electr. Power Energy Syst.*, vol. 54, pp. 244–254, Jan. 2014.

[9] S. D'Arco, J. A. Suul, and O. B. Fosso, "A virtual synchronous machine implementation for distributed control of power converters in smartgrids," *Electr. Power Syst. Res.*, vol. 122, pp. 180–197, May 2015.

[10] R. Teodorescu, M. Liserre, and P. Rodriguez, *Grid Converters for Photovoltaic and Wind Power Systems*. Sussex, U.K.: Wiley, 2011.

[11] E. Rakhshani and P. Rodriguez, "Inertia emulation in AC/DC interconnected power systems using derivative technique considering frequency measurement effects," *IEEE Trans. Power Syst.*, vol. 32, no. 5, pp. 3338–3351, Sep. 2017.

[12] H. Bevrani, *Robust Power System Frequency Control*, 2nd ed. New York, NY, USA: Springer, 2014.
[13] T. Kerdphol, F. S. Rahman, Y. Mitani, M. Watanabe, and S. Küfeoğlu, "Robust virtual inertia control of an islanded microgrid considering high penetration of renewable energy," *IEEE Access*, vol. 6, pp. 625–636, 2018.
[14] A. Fathi, Q. Shafiee, and H. Bevrani, "Robust frequency control of microgrids using an extended virtual synchronous generator," *IEEE Trans. Power Syst.*, vol. 33, no. 6, pp. 6289–6297, Nov. 2018.
[15] P. Kundur, *Power System Stability and Control*. New York, NY, USA: McGraw-Hill, 1994.
[16] H. Bevrani, M. Watanabe, and Y. Mitani, *Power System Monitoring and Control*. Hoboken, NJ, USA: Wiley, 2014.
[17] H. Bevrani, B. François, and T. Ise, *Microgrid Dynamics and Control*. Hoboken, NJ, USA: Wiley, 2017.
[18] A. R. Panel, "Stage one final determination: Review of the frequency operating standard," Austral. Energy Market Commission, Sydney, NSW, Australia, Tech. Rep. REL0065, 2017.

THONGCHART KERDPHOL (S'14–M'16) received the B.Eng. and M.Eng. degrees(Hons.) in electrical engineering from Kasetsart University, Bangkok, Thailand, in 2010 and 2012, respectively, and the Ph.D. degree in electrical and electronic engineering from the Kyushu Institute of Technology (Kyutech), Kitakyushu, Fukuoka, Japan, in 2016, where he was a Postdoctoral Fellow with the Department of Electrical and Electronic Engineering, from 2016 to 2017. In 2018, he was a Visiting Researcher with the Institute of Electrical Power Engineering and Energy Systems (IEE), Clausthal University of Technology (TU Clausthal), Clausthal-Zellerfeld, Germany. Since 2019, he has been a Senior Research Fellow with the Power System and Renewable Energy Laboratory (Mitani-Watanabe Lab), Kyutech. His research interests include power system stability, robust power system control, intelligent optimization, and smart/micro-grid control. He is also a member of the Institute of Electrical Engineers of Japan (IEEJ).

FATHIN SAIFUR RAHMAN (S'15) received the B.Sc. degree in electrical power engineering and the M.Sc. degree in electrical engineering from the Institut Teknologi Bandung, Indonesia, in 2012 and 2013, respectively. He is currently pursuing the Ph.D. degree in electrical and electronic engineering with the Mitani-Watanabe Laboratory, Kyushu Institute of Technology (Kyutech), Fukuoka, Japan.

His research interests include power system stability, smart grid and clean energy, optimization in power systems, and application of synchrophasor in power systems.

MASAYUKI WATANABE (S'03–M'05) received the B.Sc., M.Sc., and D.Eng. degrees in electrical engineering from Osaka University, Japan, in 2001, 2002, and 2004, respectively.

Since 2004, he has been with the Department of Electrical and Electronic Engineering, Kyushu Institute of Technology (Kyutech), Fukuoka, Japan, where he is currently an Associate Professor. He holds the PMU licensed patent. He has authored books/book chapters and over 100 journal/conference papers. His research interest includes the area of the analysis of power systems. He is also a member of the Institute of Electrical Engineers of Japan (IEEJ).

YASUNORI MITANI (M'87) received the B.E., M.E., and D.E. degrees from Osaka University, Osaka, Japan, in 1981, 1983, and 1986, respectively. From 1994 to 1995, he was a Visiting Research Associate with the University of California at Berkeley, Berkeley, CA, USA. He is currently a Professor, the Director of the Industry-Academic Collaboration Division, and the Vice President of the Kyushu Institute of Technology (Kyutech), Kitakyushu, Japan. He holds the PMU licensed patent. He has authored numerous books/book chapters and over 250 journal/conference papers. His research interests include the areas of power system stability, dynamics, and control. From 2016 to 2018, he served as the President of the Institute of Electrical Engineers of Japan (IEEJ), Power and Energy Society. He is also a Distinguished Lecturer of the IEEJ, Power and Energy Society.